Microstructural and Crystallographic Characterization of $Ni_{2+x}Mn_{1-x}Ga$ Alloys (x = 0.14, 0.16, 0.19, 0.22, and 0.24) by Transmission Electron Microscopy

LE ZHOU, ANIT GIRI, KYU CHO, HELGE HEINRICH, BHASKAR S. MAJUMDAR, and YONGHO SOHN

Heusler alloy, Ni_2MnGa, and its off-stoichiometric solid solutions have great potential applications in refrigeration technology due to their magnetocaloric effect (MCE), which can be strongly influenced by martensitic phase transformations and related crystallography. In this study, five polycrystalline alloys with nominal compositions of $Ni_{2+x}Mn_{1-x}Ga$ (x = 0.14, 0.16, 0.19, 0.22, and 0.24) were prepared by triple arc-melting and characterized by differential scanning calorimetry for measurement of martensitic transformation temperature, optical microscopy for microstructural observation, and X-ray diffraction and transmission electron microscopy (TEM) for detailed microstructural and crystallographic analyses. Martensitic transformation temperature was closest to room temperature for the $Ni_{2.14}Mn_{0.86}Ga$ (x = 0.14) alloy, and the transformation temperature increased with an increase in valence electron concentration (e/a). For the $Ni_{2.14}Mn_{0.86}Ga$ (x = 0.14) alloy, extensive TEM analyses confirmed the presence of modulated 7 M martensites, however, only non-modulated (NM) martensites were observed in all other alloys including $Ni_{2.16}Mn_{0.84}Ga$ (x = 0.16) alloy which exhibited a large MCE. Martensites examined by high resolution TEM were highly twinned in nature, and formed nano-scale twins within twinned microstructures.

DOI: 10.1007/s40553-014-0023-8

I. INTRODUCTION

WITH the driving force to replace conventional vapor compression cooling technology with magnetic refrigeration, increasing interests have been placed on Heusler alloy, Ni_2MnGa, and its off-stoichiometric solid solutions owing to their large magnetocaloric effect (MCE).[1] Magnetic refrigeration technology has the advantage of eliminating the greenhouse gases, enhancing cooling efficiency, and saving energy.[2,3] Compared to other magnetocaloric materials,[3] NiMnGa-based magnetocaloric alloys are inexpensive, easy to produce, and do not contain either rare earth or environmentally hazardous elements.

Isothermal entropy change, which is the figure of merit to compare MCEs in different materials, is proportional to the derivative of magnetization to temperature.[4] During the first order transformation between low temperature martensite and high temperature austenite phase, a large magnetization change is induced leading to large change in isothermal magnetic entropy. Since isothermal entropy change is proportional to the derivative of magnetization to temperature,[4] MCE at martensitic transformation temperature is very large; larger than that at ferromagnetic–paramagnetic transition.[5–7] It has been reported that by altering the composition, it is possible to bring the structural and magnetic phase transition temperatures close to each other. A very large MCE has been observed in NiMnGa-based alloys when this simultaneous structural and magnetic phase transition occurs.[1,6,8]

A better understanding of the martensitic transformation and martensitic structures is crucial in optimizing the MCE. Despite the intensive research on measurement of MCE and magnetic properties for $Ni_{2+x}Mn_{1-x}Ga$ alloys,[1,5–10] only few investigations have focused on the crystallography associated with the phase transformations. Powder X-ray diffraction (XRD) has been performed on $Ni_{2+x}Mn_{1-x}Ga$ alloys with x varying from 0.15 to 0.35, and documented the existence of non-modulated (NM) and seven-modulated (7 M, as the modulation period of the (1 1 0) planes in the austenitic phase is seven) martensite depending on the composition and heat treatment.[11] Compositional variation of martensite structures and phase transitions has been studied, by XRD and optical microscopy, by Jiang

LE ZHOU, Graduate Research Assistant, and YONGHO SOHN, Professor, are with the Department of Materials Science and Engineering and Advanced Materials Processing and Analysis Center, University of Central Florida, Orlando, FL 32816. Contact e-mail: yongho.sohn@ucf.edu ANIT GIRI, Senior Scientist, is with the Bowhead Science and Technology, Belcamp, MD 21005. KYU CHO, Materials Engineer, is with the Weapons and Materials Research Directorate, US Army Research Laboratory, Aberdeen Proving Ground, Aberdeen, MD 21005. HELGE HEINRICH, Associate Professor, is with the Department of Physics and Advanced Materials Processing and Analysis Center, University of Central Florida, P.O. Box 162385, Orlando, FL 32816. BHASKAR S. MAJUMDAR, Professor, is with the Department of Materials Science and Engineering, New Mexico Institute of Mining and Technology (NMT), Socorro, NM 87801.

Manuscript submitted March 18, 2014.
Article published online July 29, 2014

et al.[12] for arc-melted Ni_2MnGa and replacing Ga by Mn atoms where they observed 5 M, 7 M, and non-modulated martensites. Similar studies have been performed by Panda *et al.*[13] using XRD and some transmission electron microscopy (TEM) with Mn substituting for Ni for melt spun ribbons of NiMnGa alloys. Empirical relationship among martensite transformation temperature, Curie temperature, saturation magnetization, valence electron concentration (e/a), composition *etc.*, for NiMnGa alloys has been suggested by Jin *et al.*[14] *via* polynomial fitting of data. In all these studies, there are no mention of MCE and the potential influence of the structure and crystallography of the alloys, if there is any. In this investigation, we have chosen five polycrystalline $Ni_{2+x}Mn_{1-x}Ga$ ($x = 0.14$, 0.16, 0.19, 0.22, and 0.24) alloys to be examined by various techniques with an emphasis on TEM for detailed microstructural and crystallographic analyses on the martensitic phases. Magnetocaloric properties of some of the alloys ($x = 0.14$ and 0.16) have been studied already, and one of the alloys ($x = 0.16$) exhibited simultaneous structural and magnetic phase transformation at 340 K (67 °C).[1] In this study, we also attempt to explore the effects of microstructure and crystallography of martensites on the magnetocaloric property with extensive TEM analyses.

II. EXPERIMENTAL

Polycrystalline $Ni_{2+x}Mn_{1-x}Ga$ alloys with nominal compositions of $x = 0.14$, 0.16, 0.19, 0.22, and 0.24 were triple arc-melted in argon atmosphere, followed by homogenization at 1273 K (1000 °C) for 72 hours under high vacuum (10^{-6} Torr).

Differential scanning calorimetry (TA Instruments™ Q2000 DSC) with a heating/cooling rate of 10 K/min was carried out for all alloys to identify the martensitic transformation temperature. The Curie temperature (T_c) was also determined[1] from the magnetization versus temperature plot, and confirmed based on the inflection point of the DSC curves. The Curie temperatures of two alloys ($Ni_{2+x}Mn_{1-x}Ga$, where $x = 0.14$ and 0.16) were verified to coincide with the data obtained from the magnetization versus temperature plots.[1]

For each alloy, specimens with approximate size of 5 mm × 5 mm × 3 mm were sectioned, and ground to 1200-grit SiC-paper to smoothen the surface. The specimens were then subjected to conventional X-ray diffraction (XRD, Rigaku D-Max B Diffractometer) with Cu K_α radiation to determine the crystal structures and lattice parameters. The specimens were then mounted in epoxy and metallographically polished down to 0.25 μm, followed by chemical etching with Marble's Reagent to reveal the martensitic microstructure. Initial microstructural observation was carried out using optical microscopy (Olympus™ LEXT OLS-3000). The actual compositions of the five alloys were examined by X-ray energy dispersive spectroscopy (XEDS) equipped on a Zeiss™ Ultra 55 field emission scanning electron microscope (FE-SEM), and by chemical analysis *via* direct current plasma emission spectroscopy (DCPES) carried out at Luvak™ Incorporated. For the XEDS analysis, 20 random measurements were performed on each sample so as to obtain the average value with standard deviation.

TEM (FEI™ Tecnai F30 TEM) and scanning TEM equipped with high angle annular dark field (HAADF) detector, operating with accelerating voltage of 300 keV were employed to examine the details of microstructure and crystallography at room temperature. All the TEM foils were prepared *via* focus ion beam (FIB-FEI™ 200 TEM) *in situ* lift-out (INLO) technique, which is capable of selecting site-specific areas. For each alloy, up to four

Table I. Nominal Compositions (Atom Percent) and the e/a for Alloy $Ni_{2+x}Mn_{1-x}Ga$ ($x = 0.14$, 0.16, 0.19, 0.22, and 0.24), Determined by XEDS and DCPES

Alloy	Element	Nominal	XEDS	DCPES
$Ni_{2.14}Mn_{0.86}Ga$	Ni	53.50	52.91	52.93
	Mn	21.50	21.51	21.35
	Ga	25.00	25.58	25.72
	e/a	7.61	7.56	7.56
$Ni_{2.16}Mn_{0.84}Ga$	Ni	54.00	53.00	53.88
	Mn	21.00	21.13	20.48
	Ga	25.00	25.87	25.64
	e/a	7.62	7.56	7.59
$Ni_{2.19}Mn_{0.81}Ga$	Ni	54.75	53.62	54.52
	Mn	20.25	20.36	19.52
	Ga	25.00	26.02	25.96
	e/a	7.64	7.57	7.60
$Ni_{2.22}Mn_{0.78}Ga$	Ni	55.50	54.22	55.22
	Mn	19.50	19.91	19.18
	Ga	25.00	25.87	25.60
	e/a	7.67	7.59	7.63
$Ni_{2.24}Mn_{0.76}Ga$	Ni	56.00	54.65	55.99
	Mn	19.00	19.51	18.61
	Ga	25.00	25.84	25.40
	e/a	7.68	7.61	7.66

TEM foils were prepared by INLO-FIB for statistically confident TEM observations.

III. RESULTS

The starting elemental compositions of $Ni_{2+x}Mn_{1-x}Ga$ (x = 0.14, 0.16, 0.19, 0.22, and 0.24) alloys, herein referred to as nominal composition, and the actual compositions measured by XEDS and DCPES are reported in Table I, and presented in the ternary phase diagram in Figure 1. Measurements from XEDS and DCPES give similar compositions, and both have a slightly higher Ga composition than the starting nominal composition. The e/a value was also calculated, with 10 valence electrons per atom for Ni, 7 for Mn, and 3 for Ga, as presented in Table I. The e/a ratio calculated using the measured compositions *via* XEDS and DCPES vary slightly, but the e/a increases as the Ni-content increases regardless of the measurement technique.

Martensite start (M_s) and finish (M_f) and austenite start (A_s) and finish (A_f) temperatures were determined from DSC measurement as listed in Table II. Table II also lists the Curie temperature measured from magnetization curves.[1] Martensitic transformation temperature (T_m) defined as $T_m = 1/2\ (M_s + M_f)$ and austenitic transformation temperature (T_a) defined as $T_a = 1/2\ (A_s + A_f)$ are also reported in Table II. All specimens are observed to have a temperature hysteresis ($\Delta T = T_a - T_m$) between the forward and reverse martensitic transformations. These transformation temperature increased as the Ni-content increased in the $Ni_{2+x}Mn_{1-x}Ga$ (x = 0.14, 0.16, 0.19, 0.22, and 0.24) alloys, with the $Ni_{2.14}Mn_{0.86}Ga$ (x = 0.14) alloy having the T_m closest to the room temperature. Moreover, ΔT for the $Ni_{2.14}Mn_{0.86}Ga$ (x = 0.14) alloy is only 5 K, while that for other alloys is approximately 10 K. The T_c also slightly increased as the Ni-content (or x) increased. The $Ni_{2.16}Mn_{0.84}Ga$ (x = 0.16) alloy had the structural transformation and magnetic transition temperatures to be nearly identical.[1]

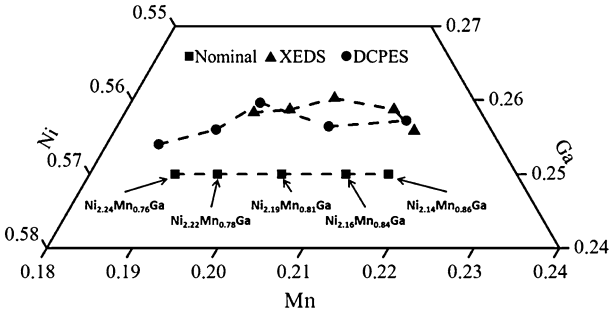

Fig. 1—Nominal compositions and measured compositions in atomic percent by XEDS and DCPES presented on the ternary phase diagram.

Figure 2 presents the XRD patterns of all alloys at room temperature. The $Ni_{2+x}Mn_{1-x}Ga$ alloys with x = 0.16, 0.19, 0.22, and 0.24 show similar XRD patterns, which can be indexed according to the NM tetragonal structure. The indexing of these patterns is based on the same crystallographic axes as of the parent austenitic phase, so that the tetragonality ratio c/a is larger than 1. The lattice parameters of a and c, as well as c/a ratio, calculated for these alloys are listed in Table III, and plotted in Figure 3 to clarify the changes in lattice parameters with the e/a. As the e/a increases (i.e., substitution of Ni for Mn), lattice parameters a slightly decreases and c increases. Therefore, the tetragonality ratio, c/a also increases as the e/a increases, which is consistent with the results reported for other NiMnGa alloys.[15,16]

The XRD pattern for the $Ni_{2.14}Mn_{0.86}Ga$ alloy with x = 0.14 is clearly different from other alloys as shown in Figure 2. The diffraction pattern is indexed according to a monoclinic unit cell, which indicates that the martensite in this alloy has a modulated 7 M crystal structure. Table III listed the lattice parameter for $Ni_{2.14}Mn_{0.86}Ga$ (x = 0.14) alloy based on the 7 M structure.

Figure 4 presents the microstructure of all alloy specimens examined by optical microscopy. The grain size for these polycrystalline specimens varied from 200 μm to 1 to 2 mm. The martensitic lamellas appear to be plate- or spear-like in shape, which is typical for shape memory alloys.[13,17] However, typical width of martensitic lamellas for the $Ni_{2.14}Mn_{0.86}Ga$ alloy appear to be smaller than that for other alloys as shown in Figure 4, with a higher density of martensitic lamellas within each grain. Similar observations have also been reported for NM and 7 M martensites with different compositions than this study.[12] Considering that the $Ni_{2.14}Mn_{0.86}Ga$ (x = 0.14) alloy has a 7 M martensite while others have NM martensites, according to XRD, it is possible that the width of a modulated martensitic variant is inherently thinner.

Figures 5(a) and (b) presents typical low and high magnification bright field (BF) TEM micrographs

Table II. Temperature (K) of the Martensite Start (M_s), Martensite Finish (M_f), Austenite Start (A_s), Austenite Finish (A_f), Martensitic Transformation (T_m), Austenitic Transformation (T_a), Curie (T_c), and Thermal Hysteresis (ΔT) Measured by DSC for the $Ni_{2+x}Mn_{1-x}Ga$ (x = 0.14, 0.16, 0.19, 0.22, and 0.24) Alloys

Alloy	M_s	M_f	T_m	A_s	A_f	T_a	T_c	$\Delta T = T_a - T_m$
$Ni_{2.14}Mn_{0.86}Ga$	313	308	310.5	313	318	315.5	335	5
$Ni_{2.16}Mn_{0.84}Ga$	336	324	330	335	347	341	339	11
$Ni_{2.19}Mn_{0.81}Ga$	350	339	344.5	349	360	354.5	358	10
$Ni_{2.22}Mn_{0.78}Ga$	428	400	414	411	435	423	375	9
$Ni_{2.24}Mn_{0.76}Ga$	431	419	425	431	445	438	372	13

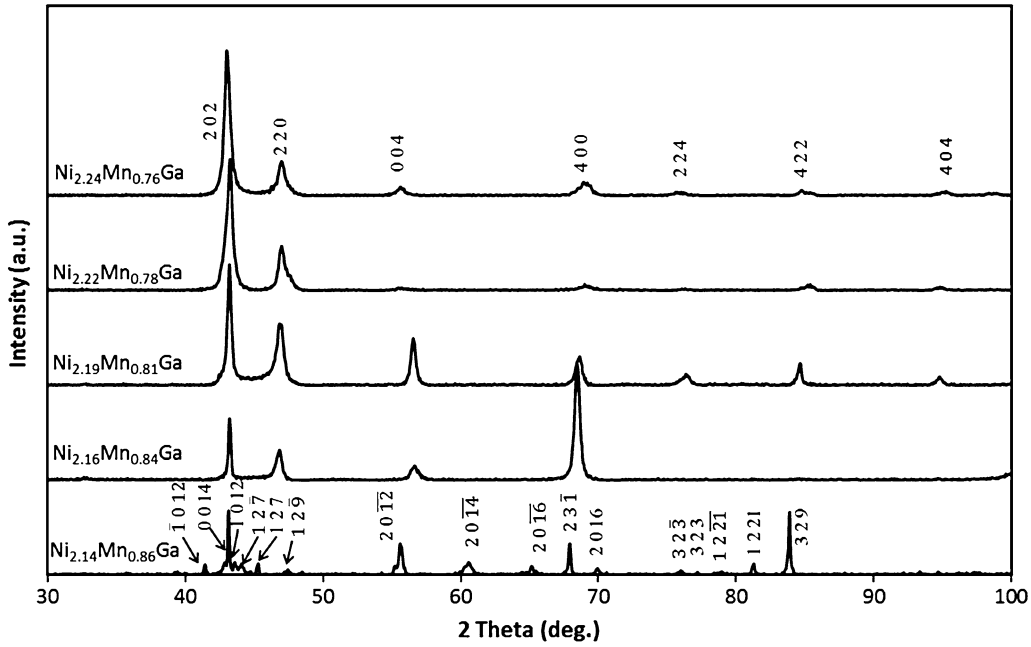

Fig. 2—X-ray diffraction patterns from the $Ni_{2+x}Mn_{1-x}Ga$ (x = 0.14, 0.16, 0.19, 0.22, and 0.24) alloys at room temperature.

Table III. Crystal Structures and Lattice Parameters (Å) for the $Ni_{2+x}Mn_{1-x}Ga$ (x = 0.14, 0.16, 0.19, 0.22, and 0.24) Alloys Determined by X-Ray Diffraction

Alloy	Crystal Structure	Space Group	a	b	c	β (deg)	c/a
$Ni_{2.14}Mn_{0.86}Ga$	7 M monoclinic	$P2/m$	4.217	5.421	29.521	92.98	
$Ni_{2.16}Mn_{0.84}Ga$	NM tetragonal	$Fmmm$	5.477		6.492		1.185
$Ni_{2.19}Mn_{0.81}Ga$	NM tetragonal	$Fmmm$	5.462		6.512		1.192
$Ni_{2.22}Mn_{0.78}Ga$	NM tetragonal	$Fmmm$	5.434		6.573		1.209
$Ni_{2.24}Mn_{0.76}Ga$	NM tetragonal	$Fmmm$	5.442		6.593		1.212

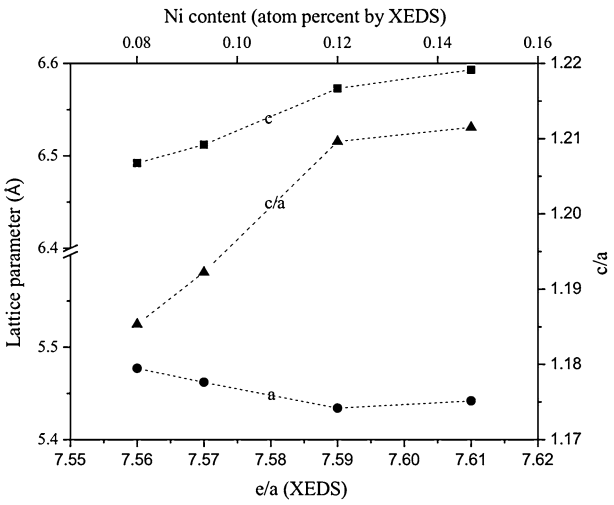

Fig. 3—Lattice parameters, a and c, and tetragonality ratio c/a determined at room temperature for the $Ni_{2+x}Mn_{1-x}Ga$ (x = 0.14, 0.16, 0.19, 0.22, and 0.24) alloys as a function of e/a.

of martensitic variants from the $Ni_{2.14}Mn_{0.86}Ga$ (x = 0.14) alloy. Selected area diffraction patterns (SADP) from a single martensitic variant and from the interface between two adjacent variants are presented in Figures 5(c) and (d), respectively. The thickness of the primary martensitic variants in this alloy varied from 100 nm to 300 nm, which is very thin and consistent with approximate observation from optical microscopy. Figure 5(b) also shows layered contrast with intervals of only a few nanometers, and indicates that the structure is modulated. Also shown in Figure 5(b) is a dark contrast at the interface between adjacent two primary variants, indicating that the boundary may be distorted. The SADP from the martensitic variant in Figure 5(c) shows six superlattice diffraction spots between the fundamental diffraction spots. Thus, the presence of modulated 7 M martensite is confirmed for the $Ni_{2.14}Mn_{0.86}Ga$ (x = 0.14) alloy. From the SADPs, the lattice parameter is determined to be a = 4.24 Å, b = 5.44 Å, c = 29.44 Å, and β = 93.2 deg for this monoclinic structure; this is quite close to that determined by XRD. The SADP with [2 1 0] zone axis from the boundary region indicates that two adjacent variants are twinned, where the twinning plane is $(1\bar{2}\bar{7})$.

High resolution TEM (HRTEM) micrographs from a single martensitic variant and from the twin boundary region were examined *via* fast Fourier transform (FFT) as presented in Figure 6. The thin-layered microstructure in Figure 6, consisting of only several atomic layers, is the modulated 7 M structure. In NiMnGa alloys, a

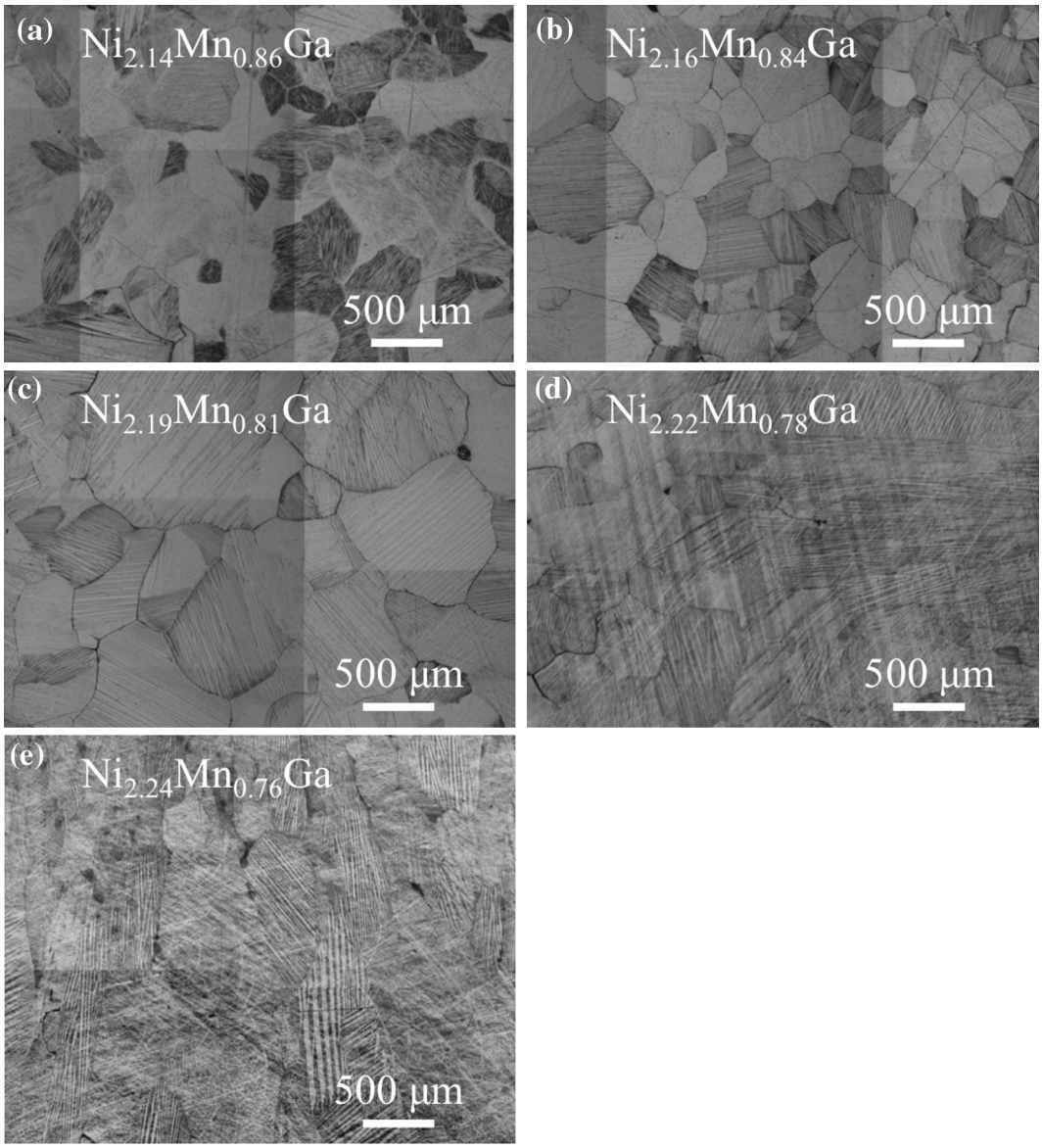

Fig. 4—Optical micrograph from martensitic microstructures for the $Ni_{2+x}Mn_{1-x}Ga$ (x = 0.14, 0.16, 0.19, 0.22, and 0.24) alloys after chemical etching.

perfect 7 M martensite typically has a $(5\bar{2})$ stacking sequence,[18,19] which forms secondary nano twins within the primary twin variants. However, the diffused spots in FFT indicate that the layered structure is locally imperfect, or some stacking faults might have been generated during the martensitic transformation. Figure 6(b) also shows the HRTEM micrograph from the boundary between two primary martensitic variants. This twin boundary appears to be not perfectly flat, with some distortion within a thickness range of a few atomic layers. This implies that the primary twin boundary is not coherent. Fast Fourier transformation from the boundary region shows that the two variants have basically the same 7 M crystal structure, as also seen from the SADP in Figure 5(d).

TEM investigation from $Ni_{2+x}Mn_{1-x}Ga$ alloys with x = 0.16, 0.19, 0.22, and 0.24 showed similar microstructure and crystal structure, but very different from the $Ni_{2.14}Mn_{0.86}Ga$ (x = 0.14) alloy. Figure 7(a) presents a typical BF TEM micrograph taken from the $Ni_{2.16}Mn_{0.84}Ga$ (x = 0.16) alloy. The width of the primary martensitic variants for these samples is typically in the range of micrometers, and thicker than that for the $Ni_{2.14}Mn_{0.86}Ga$ (x = 0.14) alloy. In Figure 7(b), the SADP taken from the interface area, with the orientation of [111], indicates that the adjacent martensitic variants are twinned, with the twinning plane of $(20\bar{2})$. However, the dark contrast seen in Figure 7(a) at the interface between adjacent primary variants indicates that this boundary is also distorted.

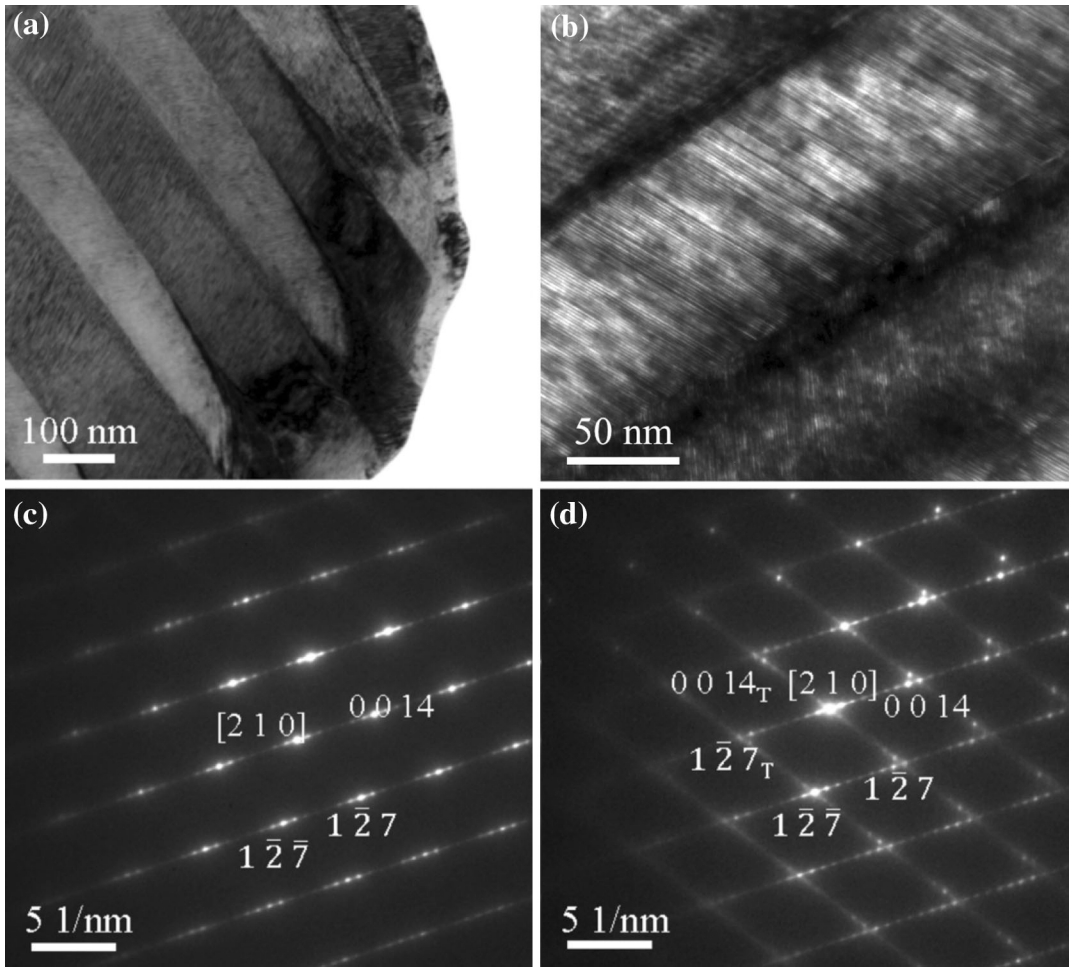

Fig. 5—(*a*) Bright field TEM micrograph from the $Ni_{2.14}Mn_{0.86}Ga$ alloy showing the martensitic variants. (*b*) Bright field TEM micrograph from the twin variants and boundary. Selected area diffraction patterns of the $Ni_{2.14}Mn_{0.86}Ga$ alloy from (*c*) individual martensitic variant and (*d*) twin boundary region.

Figure 7(a) also reveals that, within each primary martensitic variant, thinner secondary twin variants with straight boundaries exist. Figure 8 demonstrates by HR-TEM, taken from the orientation of [1 1 1], that the thickness of these secondary twins varies from 10 to 20 nm, and lead to some diffuse scattering in the corresponding FFT. The FFT also shows a similar pattern to the SADP taken from the twin boundary area at the orientation of [1 1 1]. Therefore, these secondary nanotwins in NM martensites have the same orientation relationship as in the primary twins, where the twinning plane is the same, $(20\bar{2})$, as highlighted in Figure 8.

IV. DISCUSSION

Both NM and 7 M martensites formed hierarchical twins-secondary twins within the primary twins. Secondary twins form at the habit plane so as to minimize the lattice elastic strain energy during the austenite-to-martensite transformation. For both NM and 7 M martensites, the coherency of the primary twin boundary was lost, corresponding to higher boundary energy for the primary twin variants. The primary twin variants with different alignment with respect to the secondary twins were also observed in this study, despite their higher boundary energy. Formation of the primary twin variants can help reduce the strains perpendicular to the habit plane during phase transformation.[20]

There are microstructural differences between 7 M and NM martensites. In 7 M martensites, the secondary twins have a width of a few atomic layers, and the primary twins have a width of a few hundred nanometers, as seen in Figures 5 and 6, respectively. For the NM martensites, the width for the secondary twins is about 10 to 20 nm and that for the primary twins is in the micrometer scales, as shown in Figures 7 and 8, respectively. Clearly, the thickness of the twins in 7 M martensites is thinner than that in the NM martensites, and correspond to a higher number of twin boundaries. Li *et al.*[21,22] previously reported that 7 M martensite had thinner lamellas compared to the NM martensite in a polycrystalline NiMnGa alloy, in which the 7 M martensite, NM martensite and austenite coexisted in one grain. Thus it is plausible that the twin boundary energy for the 7 M martensite is lower than that for the

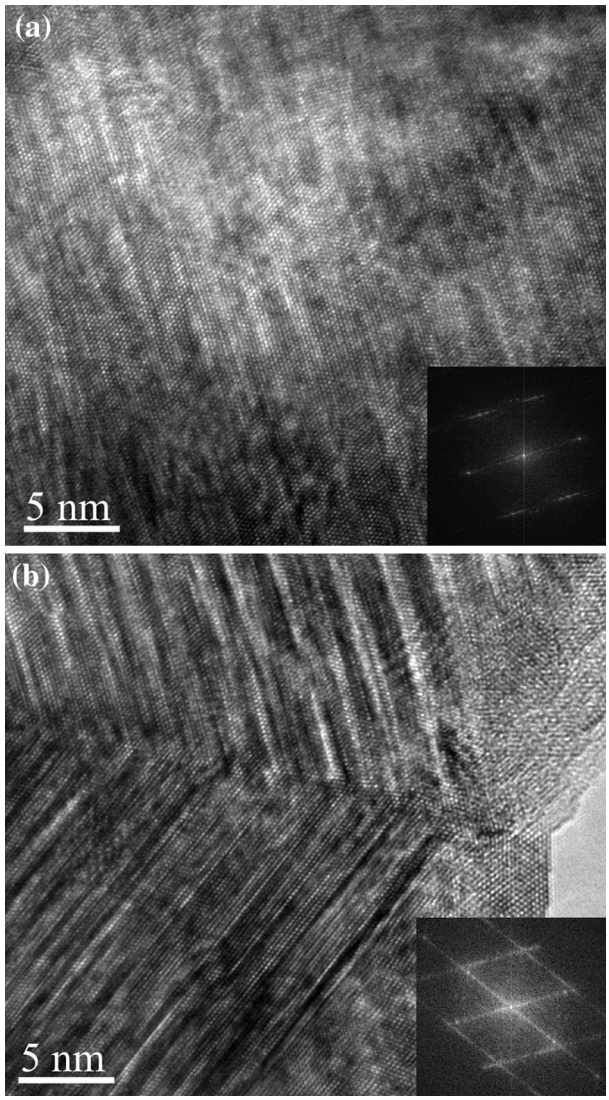

Fig. 6—High resolution TEM micrographs and corresponding fast Fourier transform patterns from the $Ni_{2.14}Mn_{0.86}Ga$ alloy: (*a*) individual martensitic variant and (*b*) twin boundary region.

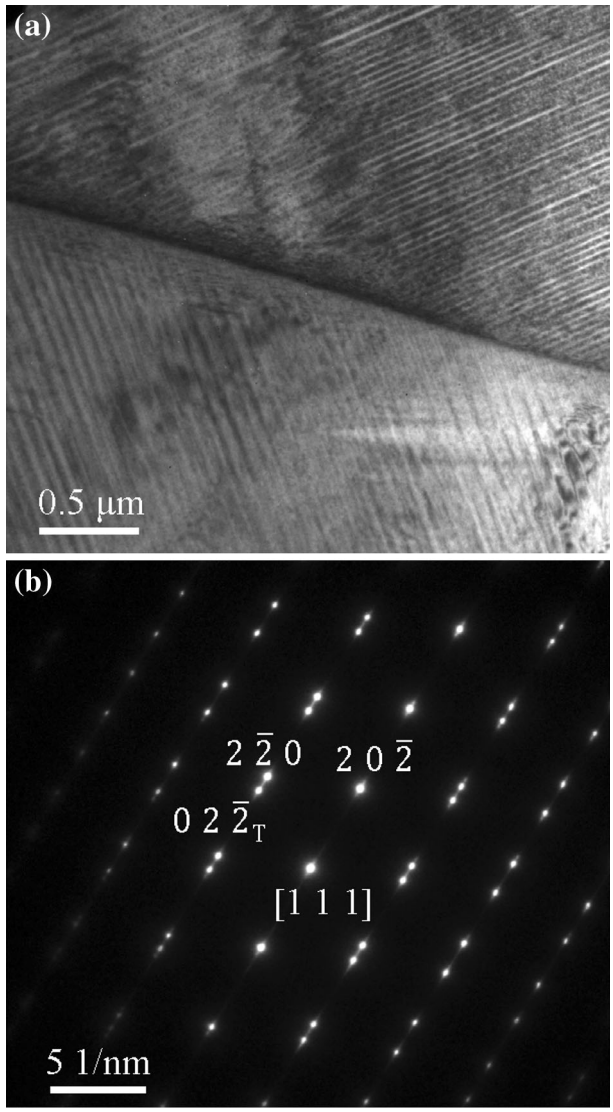

Fig. 7—(*a*) Bright field TEM micrograph of martensitic variants from $Ni_{2.16}Mn_{0.84}Ga$ alloy and (*b*) the corresponding selected area diffraction pattern from [1 1 1] orientation at the twin boundary region.

NM martensite. During martensitic transformation, more twin boundaries can form in 7 M martensite so as to further minimize the transformation strain at the habit plane. Also, lower temperature may favor the formation of 7 M martensites because of its lower twin boundary energy. This may account for why the M_s for transformation from austenite to 7 M martensite is lower than that for transformation from austenite to NM martensite, as observed in this study and in other NiMnGa alloys.[23]

As reported earlier, the MCE for $Ni_{2.16}Mn_{0.84}Ga$ ($x = 0.16$) is higher than that for $Ni_{2.14}Mn_{0.86}Ga$ ($x = 0.14$) due to the concurrence of structural and magnetic transformation. The crystal structures of the martensite for these two alloys are very different, one being the modulated structure and the other non-modulated structure. The transformation to a modulated structure might be directly related to the low thermal hysteresis as observed in $Ni_{2.14}Mn_{0.86}Ga$ ($x = 0.14$) as shown in Table II. The small twin width and high density of twins in the 7 M martensites can reduce the interfacial energy during phase transformation, and leads to a smaller hysteresis.[20,24] The small hysteresis is beneficial to a reduction in energy loss.[24] Further studies are being carried out to elucidate whether one structure is superior to the other with respect to MCE properties.

V. SUMMARY

A series of $Ni_{2+x}Mn_{1-x}Ga$ ($x = 0.14$, 0.16, 0.19, 0.22, and 0.24) polycrystalline alloys were prepared and characterized for microstructural and crystallographic analyses. Martensitic transformation temperatures were found to increase with an increase of e/a, and $Ni_{2.16}Mn_{0.84}Ga$ alloy had the closest transition temperature to the room temperature. While modulated 7 M

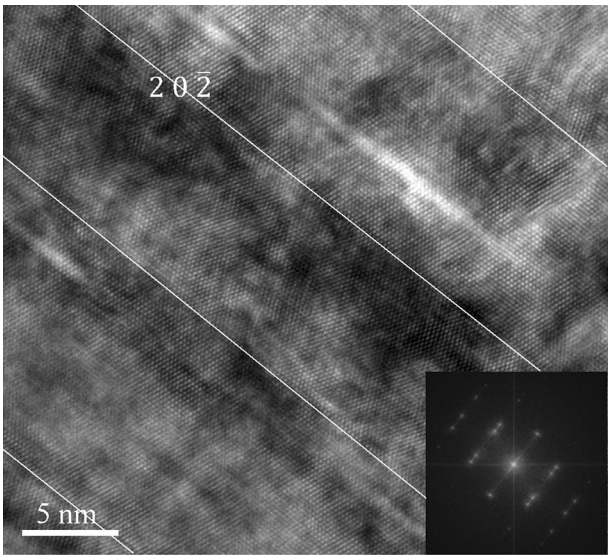

Fig. 8—High resolution TEM micrograph and corresponding fast Fourier transform pattern from the $Ni_{2.16}Mn_{0.84}Ga$ alloy.

martensites were observed in $Ni_{2.14}Mn_{0.86}Ga$ alloy, only the NM martensites were found in all other alloys at room temperature. The lattice parameters for the NM martensites were determined by XRD, and the c/a ratio was found to increase with an increase in e/a ratio. Both NM and 7 M martensites consisted of twin variants with different orientations. The thickness of the variants in 7 M martensites was smaller than that for NM martensites. For NM martensites, the primary twin variant thickness was in the micrometer scale, and each variant consisted of very fine secondary twin variants with a thickness of few tens of nanometer. For 7 M martensites, the primary twin variant thickness was in the nanometer scale, and the variant consisted of very fine structure that has only a few atomic layers corresponding to the structural modulation.

ACKNOWLEDGMENTS

This research was sponsored by the U.S. Army Research Laboratory through cooperative agreement #W911NF-11-2-0020 between University of Central Florida and the U.S. Army Research Laboratory. The authors would also like to thank Pittsburgh Materials Technology Incorporated for preparation of the alloys.

REFERENCES

1. A.K. Giri, B.A. Paterson, M.V. McLeod, C.L. Dennis, B.S. Majumdar, K.C. Cho, and R.D. Shull: *J. Appl. Phys.*, 2013, vol. 113, p. 17A907.
2. O. Tegus, E. Brück, K. Buschow, and F. De Boer: *Nature*, 2002, vol. 415, pp. 150–52.
3. V. Franco, J.S. Blazquez, B. Ingale, and A. Conde: *Annu. Rev. Mater. Res.*, 2012, vol. 42, pp. 305–42.
4. V.K. Pecharsky and K.A. Gschneidner, Jr: *J. Magn. Magn. Mater.*, 1999, vol. 200, pp. 44–56.
5. F. Hu, B. Shen, and J. Sun: *Appl. Phys. Lett.*, 2000, vol. 76, pp. 3460–62.
6. L. Pareti, M. Solzi, F. Albertini, and A. Paoluzi: *Eur. Phys. J. B*, 2003, vol. 32, pp. 303–07.
7. F. Hu, B. Shen, J. Sun, and G. Wu: *Phys. Rev. B*, 2001, vol. 64, pp. 132412–15.
8. V. Khovaylo, V. Buchelnikov, R. Kainuma, V. Koledov, M. Ohtsuka, V. Shavrov, T. Takagi, S. Taskaev, and A. Vasiliev: *Phys. Rev. B*, 2005, vol. 72, p. 224408.
9. V. Buchelnikov, V. Sokolovskiy, H. Herper, H. Ebert, M. Gruner, S. Taskaev, V. Khovaylo, A. Hucht, A. Dannenberg, and M. Ogura: *Phys. Rev. B*, 2010, vol. 81, p. 094411.
10. M. Pasquale, C. Sasso, L. Lewis, L. Giudici, T. Lograsso, and D. Schlagel: *Phys. Rev. B*, 2005, vol. 72, p. 094435.
11. S. Banik, R. Ranjan, A. Chakrabarti, S. Bhardwaj, N. Lalla, A. Awasthi, V. Sathe, D. Phase, P. Mukhopadhyay, and D. Pandey: *Phys. Rev. B*, 2007, vol. 75, p. 104107.
12. C. Jiang, Y. Muhammad, L. Deng, W. Wu, and H. Xu: *Acta Mater.*, 2004, vol. 52, pp. 2779–85.
13. A. Panda, S. Singh, R.K. Roy, M. Ghosh, and A. Mitra: *J. Magn. Magn. Mater.*, 2011, vol. 323, pp. 1161–69.
14. X. Jin, M. Marioni, D. Bono, S. Allen, R. O'Handley, and T. Hsu: *J. Appl. Phys.*, 2002, vol. 91, pp. 8222–24.
15. C. Jiang, G. Feng, S. Gong, and H. Xu: *Mater. Sci. Eng. A*, 2003, vol. 342, pp. 231–35.
16. V. Chernenko, V. L'vov, E. Cesari, J. Pons, R. Portier, and S. Zagorodnyuk: *Mater. Trans.*, 2002, vol. 43, pp. 856–60.
17. M. Nishida, T. Hara, M. Matsuda, and S. Ii: *Mater. Sci. Eng. A*, 2008, vol. 481, pp. 18–27.
18. J. Pons, V. Chernenko, R. Santamarta, and E. Cesari: *Acta Mater.*, 2000, vol. 48, pp. 3027–38.
19. J. Pons, R. Santamarta, V. Chernenko, and E. Cesari: *Mater. Sci. Eng. A*, 2006, vol. 438, pp. 931–34.
20. S. Kaufmann, R. Niemann, T. Thersleff, U.K. Rößler, O. Heczko, J. Buschbeck, B. Holzapfel, L. Schultz, and S. Fähler: *New J. Phys.*, 2011, vol. 13, p. 053029.
21. Z Li, Y Zhang, C. Esling, X Zhao, and L Zuo: *Acta Mater.*, 2012, vol. 60, pp. 6982–90.
22. Z Li, N Xu, Y Zhang, C. Esling, j.-M. Raulot, X Zhao, and L Zuo: *Acta Mater.*, 2013, vol. 61, pp. 3858–65.
23. N. Lanska, O. Soderberg, A. Sozinov, Y. Ge, K. Ullakko, and V. Lindroos: *J. Appl. Phys.*, 2004, vol. 95, pp. 8074–78.
24. R. Niemann, U.K. Rößler, M.E. Gruner, O. Heczko, L. Schultz, and S. Fähler: *Adv. Eng. Mater.*, 2012, vol. 14, pp. 562–81.